

Distribution of fidelity zeros in two-band topological models

Siyan Lin,^{1,2} Zhen-Yu Zheng,¹ and Shu Chen^{1,2,*}

¹*Beijing National Laboratory for Condensed Matter Physics,*

Institute of Physics, Chinese Academy of Sciences, Beijing 100190, China

²*School of Physical Sciences, University of Chinese Academy of Sciences, Beijing 100049, China*

(Dated: March 20, 2026)

We investigate the distribution of fidelity zeros in two-band topological models by extending the phase transition driving parameter into the complex plane. Within the biorthogonal formulation, we unveil that fidelity zeros are related to momentum modes for which the real part of the energy gap vanishes. Guided by this relation, we analyze the Kitaev chain, the Haldane model, and the Qi-Wu-Zhang (QWZ) model. In finite-size systems the zeros form discrete lines parallel to the imaginary axis, while in the thermodynamic limit they accumulate into extended regions in the complex parameter plane. For the Kitaev and Haldane models, the accessible interval of the real part of the complexified parameter is bounded by the critical points of the corresponding topological transitions. For the QWZ model, the transitions at $u = \pm 2$ are identified in the same way, whereas the critical point at $u = 0$ is signaled by fidelity zeros crossing the real axis. These results extend the fidelity-zero framework to topological quantum phase transitions and clarify how critical information is encoded in complexified parameter space.

I. INTRODUCTION

The study of quantum phase transitions [1] has always been a central topic in modern condensed matter physics. These transitions, driven by quantum fluctuations at zero temperature, signify qualitative changes in the ground-state properties of a quantum system. Therefore, the ground-state fidelity, which measures the overlap between ground states at different parameters, naturally encodes the information of quantum criticality. Fidelity and fidelity susceptibility have emerged as powerful, widely employed diagnostics for detecting quantum critical points, achieving remarkable success across a broad range of models [2–9].

Recently, inspired by Loschmidt echo zeros in dynamical quantum phase transitions [10–21], the concept of fidelity zeros has been proposed to probe quantum phase transitions [22]. To overcome the Anderson orthogonality catastrophe, Ref. [22] employed twist boundary conditions (tunable via a magnetic flux ϕ), demonstrating that an exact fidelity zero can be accessed for states in different phases by tuning ϕ , while no zero exists for states in the same phase. This scheme, however, operates entirely within the real parameter space of the Hamiltonian.

A more fundamental extension, in the spirit of the Lee-Yang theory [23–32], was subsequently developed by extending the Hamiltonian parameter into the complex plane [33, 34]. In this framework, fidelity zeros emerge naturally in the complex-extended parameter space, and their location obeys a Lee-Yang-type theorem, offering a unified diagnostic for quantum criticality. This formulation has been successfully applied to symmetry-breaking phase transitions such as the quantum Ising model and the clock models. In such models, fidelity zeros emerge

exclusively within one phase, disappear abruptly at the critical point. Refs. [33, 34] attribute such behaviors to non-Hermitian parity-symmetry breaking.

However, whether this fidelity-zero framework can be applied to topological systems remains an open question. Topological quantum phase transitions involve changes in global topological invariants without local order parameters or spontaneous symmetry breaking. The mechanism of non-Hermitian symmetry breaking, central to prior demonstrations, is not directly applicable to topological systems. It is interesting to scrutinize topological quantum phase transitions in the fidelity-zero framework and clarify how critical information is encoded in complexified parameter space.

In this work, we study fidelity zeros in two-band topological models. We demonstrate that fidelity zeros emerge in the complex parameter plane precisely when the real part of the energy gap closes for specific momentum modes. Using the Kitaev chain, the Haldane model, and the Qi-Wu-Zhang (QWZ) model as paradigmatic examples, we investigate the distribution of fidelity zeros and find these zeros display similar patterns: these zeros are distributed along lines parallel to the imaginary axis in finite-size systems, with their real parts confined to a finite interval. Importantly, as the system approaches the thermodynamic limit, the boundaries of this interval converge and ultimately correspond to the critical points of the topological quantum phase transition. We establish that the presence or absence of fidelity zeros reliably signals the topological phase boundary, indicating that the fidelity-zero approach offers a powerful tool for probing topological quantum phase transitions.

* Corresponding author: schen@iphy.ac.cn

II. FIDELITY ZEROS AND THEIR CONNECTION TO THE ENERGY SPECTRUM

Fidelity zeros are analogous to Lee-Yang zeros, which are distributed in the complex plane. To explore such zeros, it is necessary to extend at least one parameter of the Hamiltonian into the complex domain, thereby rendering the Hamiltonian non-Hermitian. The non-Hermiticity leads to two important consequences. First, since the eigenenergies are generally complex, the concept of a “ground state” is defined with respect to the real part of the energy; the state with the smaller real part is identified as the lower-energy state. Second, the calculation of fidelity should be formulated using the biorthogonal basis [35] constructed from the left and right eigenstates.

We consider a generic two-band system with the momentum-space Hamiltonian expressed as

$$H_k(\gamma) = d_k^0(\gamma)\mathbb{I}_2 + \sum_{\beta=1}^3 d_k^\beta(\gamma)\sigma_\beta, \quad (1)$$

where σ_β ($\beta = 1, 2, 3$) is the Pauli matrix, \mathbb{I}_2 is the 2×2 identity matrix, and γ is a phase transition driving parameter. The energy spectrum of this two-band model is given by

$$E_{k,\pm}(\gamma) = d_k^0(\gamma) \pm \sqrt{\sum_{\beta=1}^3 d_k^\beta(\gamma)^2}, \quad (2)$$

and the corresponding right eigenstates can be denoted as

$$|\Psi_{k,\pm}^R(\gamma)\rangle = \frac{1}{\sqrt{|d_k^3 + E_{k,\pm}|^2 + |d_k^1 + id_k^2|^2}} \begin{pmatrix} d_k^3 + E_{k,\pm} \\ d_k^1 + id_k^2 \end{pmatrix}. \quad (3)$$

Due to the complex nature of the spectrum, it is not *a priori* evident whether $|\Psi_{k,+}^R(\gamma)\rangle$ or $|\Psi_{k,-}^R(\gamma)\rangle$ corresponds to the lower-energy state. We therefore denote the right eigenstate with the smaller (larger) real part of energy as $|\Psi_{k,g(e)}^R(\gamma)\rangle$. Similarly, we introduce the left eigenstates satisfying

$$H_k^\dagger(\gamma)|\Psi_{k,\pm}^L(\gamma)\rangle = E_{k,\pm}^*(\gamma)|\Psi_{k,\pm}^L(\gamma)\rangle, \quad (4)$$

and denote the lower- (higher-) energy left eigenstate as

$$\begin{aligned} & \langle \Psi_{k,g}^L(\gamma_0 + \delta\gamma/2) | \Psi_{k,g}^R(\gamma_0 - \delta\gamma/2) \rangle \langle \Psi_{k,g}^L(\gamma_0 - \delta\gamma/2) | \Psi_{k,g}^R(\gamma_0 + \delta\gamma/2) \rangle \\ & = \langle \Psi_{k,+}^L(\gamma_0 + \delta\gamma/2) | \Psi_{k,-}^R(\gamma_0 - \delta\gamma/2) \rangle \langle \Psi_{k,-}^L(\gamma_0 - \delta\gamma/2) | \Psi_{k,+}^R(\gamma_0 + \delta\gamma/2) \rangle. \end{aligned} \quad (8)$$

In the limit $\delta\gamma \rightarrow 0$, this overlap approaches

$|\Psi_{k,g(e)}^L(\gamma)\rangle$. The left and right eigenstates are normalized as

$$\langle \Psi_{k,\pm}^R(\gamma) | \Psi_{k,\pm}^R(\gamma) \rangle = \langle \Psi_{k,\pm}^L(\gamma) | \Psi_{k,\pm}^L(\gamma) \rangle = 1. \quad (5)$$

Given the non-Hermitian nature of the Hamiltonian, the fidelity is evaluated within the biorthogonal framework [36]. Consequently, the fidelity factorizes over momentum modes as [37, 38]

$$\mathcal{F}(\tilde{\gamma}, \gamma) = \prod_k \sqrt{|\langle \Psi_{k,g}^L(\tilde{\gamma}) | \Psi_{k,g}^R(\gamma) \rangle \langle \Psi_{k,g}^L(\gamma) | \Psi_{k,g}^R(\tilde{\gamma}) \rangle|}. \quad (6)$$

In the thermodynamic limit, the many-body fidelity always approaches zero, which can be attributed to the Anderson orthogonality catastrophe [39, 40]. To reliably identify genuine zeros in large but finite systems, we therefore introduce the minimum single-mode fidelity

$$\begin{aligned} & \mathcal{F}_{\min}(\tilde{\gamma}, \gamma) \\ & = \min_k \left[\sqrt{|\langle \Psi_{k,g}^L(\tilde{\gamma}) | \Psi_{k,g}^R(\gamma) \rangle \langle \Psi_{k,g}^L(\gamma) | \Psi_{k,g}^R(\tilde{\gamma}) \rangle|} \right], \end{aligned} \quad (7)$$

where k takes discrete values for a finite-size system. This quantity isolates the momentum mode that contributes the smallest overlap. Since the total many-body fidelity is a product over all momentum modes [Eq. (6)], the vanishing of a single factor suffices to force the total fidelity to zero. Thus, a zero in \mathcal{F}_{\min} serves as a precise indicator for genuine zeros of the total many-body fidelity.

We now elucidate the fundamental connection between the emergence of fidelity zeros and the spectral properties of the non-Hermitian Hamiltonian. A fidelity zero between two infinitesimally close parameters, $\mathcal{F}(\gamma + \delta\gamma/2, \gamma - \delta\gamma/2) \rightarrow 0$, signals a non-analyticity in the ground state at the point γ . This non-analyticity is directly triggered when, for some momentum k , the real part of the energy gap closes, i.e., $\text{Re}[E_{k,+}(\gamma) - E_{k,-}(\gamma)] = 0$. At such a point, denoted as γ_0 , the two eigenstates $|\Psi_{k,\pm}^{R(L)}(\gamma_0)\rangle$ become degenerate in their real part of the energy. Consequently, the identification of the ground-state changes discontinuously as the parameter crosses γ_0 . The state with the lower real part switches from, for instance, $|\Psi_{k,-}^{R(L)}\rangle$ (for $\gamma = \gamma_0 - \delta\gamma/2$) to $|\Psi_{k,+}^{R(L)}\rangle$ (for $\gamma = \gamma_0 + \delta\gamma/2$). The fidelity factor for this momentum mode, evaluated between states on opposite sides of γ_0 , therefore involves the overlap

$\langle \Psi_{k,+}^L(\gamma_0) | \Psi_{k,-}^R(\gamma_0) \rangle \langle \Psi_{k,-}^L(\gamma_0) | \Psi_{k,+}^R(\gamma_0) \rangle$, which is zero

due to the biorthogonality of the eigenstates. Therefore, we demonstrate that a genuine fidelity zero emerges precisely when the real part of the energy gap closes, i.e., $\text{Re}[E_{k,+}(\gamma) - E_{k,-}(\gamma)] = 0$, for a specific momentum mode k .

Based on this intrinsic connection between fidelity zeros and the energy spectrum, we introduce the minimum real part of the energy gap

$$E_{\min}(\gamma) = \min_{k \in \text{1BZ}} |\text{Re}(E_{k,+} - E_{k,-})|, \quad (9)$$

where k takes values in the first Brillouin zone (1BZ) continuously. A necessary condition for the occurrence of a fidelity zero at some $\gamma = \gamma_0$ is that $E_{\min}(\gamma_0) = 0$, i.e., the real part of the energy gap must vanish for at least one momentum mode. However, we emphasize that the converse is not automatically guaranteed in a finite-size system. Because the momenta are discrete in a finite-size system, e.g., $k = 2\pi m/L$ with $m = 0, 1, \dots, L/2$ for the Kitaev chain, the actual minimum over the discrete set, $\min_{\text{discrete } k} |\text{Re}(E_{k,+} - E_{k,-})|$, may remain nonzero even at parameters where $E_{\min}(\gamma) = 0$ holds. Consequently, while the condition $E_{\min}(\gamma) = 0$ gives the locations of fidelity zeros in the thermodynamic limit, it is a necessary but not sufficient condition for their appearance in finite-size systems.

III. DISTRIBUTION OF FIDELITY ZEROS

In this section, we investigate the distribution of fidelity zeros for some typical topological models via the minimum real part of the energy gap [Eq. (9)] and the minimum single-mode fidelity [Eq. (7)].

A. Kitaev chain

First, we consider the one-dimensional Kitaev chain [41], a paradigmatic model for topological superconductivity. Its Hamiltonian can be cast into the standard two-band form of Eq. (1) with the components

$$d_k^0 = d_k^1 = 0, \quad d_k^2 = -\Delta \sin k, \quad d_k^3 = -\mu - t \cos k, \quad (10)$$

where t is the hopping amplitude, μ is the on-site chemical potential, and Δ denotes the amplitude of p-wave superconducting pairing. For simplicity, we set $t = 1$. The energy spectrum is given by

$$E_{k,\pm}(\mu) = \pm \sqrt{(\mu + \cos k)^2 + (\Delta \sin k)^2}. \quad (11)$$

For a system of size L , the allowed momenta are given by $k = 2\pi m/L$ with $m = 0, 1, \dots, L/2$, where we assume L to be even.

The topology of the Kitaev chain is characterized by the winding number ν . The model undergoes topological

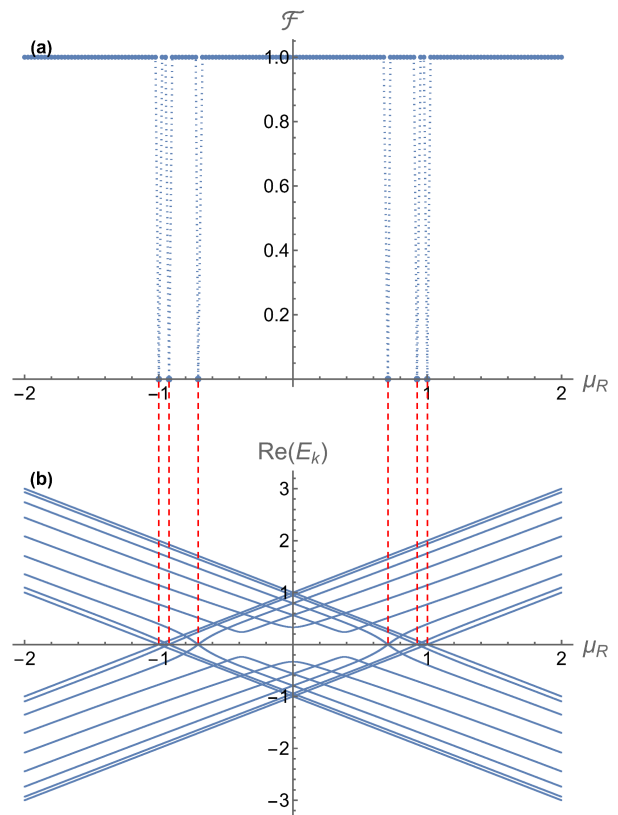


FIG. 1. (a) Fidelity $\mathcal{F}(\mu + \delta\mu/2, \mu - \delta\mu/2)$ and (b) the real part of the eigenenergies $\text{Re}(E_{k,\pm})$ as a function of μ_R , with fixed $\Delta = 0.6$, $\mu_I = 0.5$, $\delta\mu = 0.001(1 + i)$ and $L = 16$. The positions where $\text{Re}(E_{k,\pm})$ vanishes coincide precisely with the fidelity zeros, as indicated by the red dashed lines.

quantum phase transitions at

$$\mu = \pm 1 \quad (\text{for } \Delta \neq 0). \quad (12)$$

The system resides in a topologically non-trivial phase with $\nu = 1$ for $|\mu| < 1$, and in a topologically trivial phase with $\nu = 0$ for $|\mu| > 1$.

To explicitly verify the connection between fidelity zeros and the energy spectrum, we extend the chemical potential into the complex plane, setting $\mu = \mu_R + i\mu_I$. We then compute both the ground-state fidelity $\mathcal{F}(\mu + \delta\mu/2, \mu - \delta\mu/2)$ and the real part of the eigenenergies $\text{Re}(E_k)$ along a chosen path in the complex μ -plane. Here we fix $\mu_I = 0.5$ and vary μ_R [see the green dashed line in Fig. 2(b)]. As shown in Fig. 1(a), the fidelity remains a constant value of 1 except at some specific parameter values, where sharp dips or zeros of the fidelity are clearly visible. These zeros coincide precisely with the points where the real part of the energy gap closes, as indicated by the red dashed lines in Fig. 1. This one-to-one correspondence confirms the argument presented earlier: a fidelity zero emerges if and only if the real part of the energy gap closes for at least one momentum mode. Besides, fidelity zeros are confined within the interval $|\mu_R| \leq 1$. The boundaries of this interval give rise

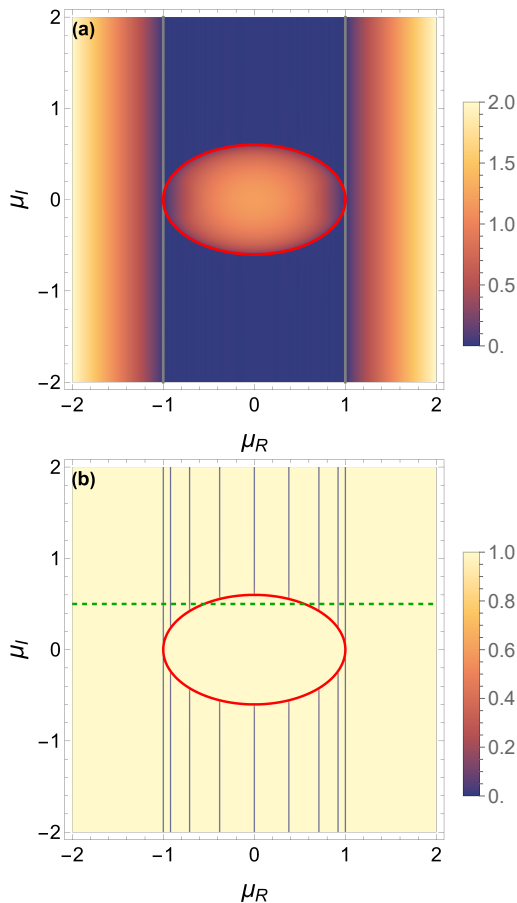


FIG. 2. (a) The minimum real part of the energy gap $E_{\min}(\mu)$ and (b) the minimum single-mode fidelity $\mathcal{F}_{\min}(\mu + \delta\mu/2, \mu - \delta\mu/2)$ as a function of μ in the complex plane for the Kitaev chain. We fix $\Delta = 0.6$ for both panels. In panel (b) we fix $\delta\mu = 0.01(1 + i)$ and $L = 16$.

to the topological quantum phase transition points.

Next, we examine the distribution of fidelity zeros in the complex μ -plane. In Fig. 2(a) we plot the minimum real part of the energy gap $E_{\min}(\mu)$ for $\Delta = 0.6$. It is shown that there exists a region where $E_{\min}(\mu) = 0$, with boundaries indicated by the red closed curve and gray lines. Importantly, the gray lines are located at $|\mu_R| = 1$, coinciding with the critical points of the underlying topological quantum phase transition. For $|\mu_R| > 1$, $E_{\min}(\mu)$ is strictly positive, indicating the absence of fidelity zeros in that region. The red curve can be determined analytically by solving

$$E_{k,\pm}(\mu) = \pm \sqrt{(\mu + \cos k)^2 + (\Delta \sin k)^2} = 0, \quad (13)$$

which yields the parametric form

$$\mu = -\cos k \pm i\Delta \sin k. \quad (14)$$

Consequently, the region where $E_{k,\pm}(\mu) = 0$ is given by

$$R = \left\{ \mu = \mu_R + i\mu_I : |\mu_R| \leq 1, \mu_R^2 + \left(\frac{\mu_I}{\Delta}\right)^2 \geq 1 \right\}. \quad (15)$$

We now turn to the numerical detection of fidelity zeros, using the minimum single-mode fidelity \mathcal{F}_{\min} defined in Eq. (7). In Fig. 2(b) we plot \mathcal{F}_{\min} in the complex μ -plane. The dark blue lines are identified as the fidelity zeros. These fidelity zeros lie in the region R as expected, and are distributed along lines parallel to the imaginary axis. The distribution of fidelity zeros can be obtained analytically, by requiring the real part of the energy gap to vanish, i.e. $\text{Re}(E_{k,+}(\mu) - E_{k,-}(\mu)) = 0$. This is equivalent to the condition

$$(\mu + \cos k)^2 + (\Delta \sin k)^2 \leq 0. \quad (16)$$

Substituting $\mu = \mu_R + i\mu_I$ into this inequality and expanding the left-hand side, we obtain

$$\begin{aligned} \mu_R^2 - \mu_I^2 + \cos^2 k + 2\mu_R \cos k + (\Delta \sin k)^2 \\ + 2i(\mu_R + \cos k)\mu_I \leq 0. \end{aligned} \quad (17)$$

The real part and imaginary part give two separate constraints

$$\begin{aligned} \mu_R^2 - \mu_I^2 + \cos^2 k + 2\mu_R \cos k + (\Delta \sin k)^2 \leq 0, \\ 2(\mu_R + \cos k)\mu_I = 0. \end{aligned} \quad (18)$$

For a finite-size system with discrete momenta $k = 2\pi m/L$ ($m = 0, 1, \dots, L/2$), these constraints yields the explicit locations of fidelity zeros

$$\mu_R = -\cos\left(\frac{2\pi m}{L}\right) \quad \left(m = 0, 1, \dots, \frac{L}{2}\right), \quad (19a)$$

$$\mu_R^2 + \left(\frac{\mu_I}{\Delta}\right)^2 \geq 1, \quad (19b)$$

Crucially, the occurrence of these zeros depends sharply on the real part μ_R of the complexified parameter. For $|\mu_R| > 1$, no zeros appear, whereas for $|\mu_R| \leq 1$ zeros are present. This abrupt change in the zero pattern precisely at $|\mu_R| = 1$ provides a strong indication of the topological quantum phase transition in the original Hermitian Kitaev chain, where the critical points are located at $\mu = \pm 1$. Thus, monitoring the existence of fidelity zeros as a function of μ_R offers a diagnostic of the underlying quantum phase transition.

Moreover, we note that the Su-Schrieffer-Heeger (SSH) model [42, 43] can be viewed as a special case of the Kitaev chain with $\Delta = t$ after a suitable rotation of the vector \mathbf{d}_k . The Hamiltonian of the SSH model takes the form of Eq. (1) with the components

$$d_k^0 = d_k^3 = 0, \quad d_k^1 = t_1 + t_2 \cos k, \quad d_k^2 = t_2 \sin k, \quad (20)$$

where t_1 and t_2 are intra-cell and inter-cell hopping amplitudes, respectively. By performing a $\pi/2$ rotation

around the d_k^2 -axis and identifying $\mu = -t_1$, $\Delta = t = -t_2$, one recovers the Kitaev chain. Consequently, the analysis of fidelity zeros for the SSH model follows directly from the Kitaev chain results. For simplicity, we fix $t_2 = -1$ and extend t_1 into the complex plain, $t_1 = t_{1R} + it_{1I}$. Then fidelity zeros are located at

$$t_{1R} = \cos\left(\frac{2\pi m}{L}\right), \quad \left(m = -\frac{L}{2} + 1, -\frac{L}{2} + 2, \dots, \frac{L}{2}\right) \quad (21a)$$

$$t_{1R}^2 + t_{1I}^2 \geq 1. \quad (21b)$$

From Eq. (21a) we can directly deduce $|t_{1R}| \leq 1$. The

boundaries exactly give rise to the critical points of the SSH model.

B. Haldane model

Next, we examine fidelity zeros in the Haldane model on a honeycomb lattice [44], a paradigmatic example of a Chern insulator that exhibits the quantum anomalous Hall effect. Its Bloch Hamiltonian can be written in the standard two-band form of Eq. (1) with the components

$$\begin{aligned} d_{\mathbf{k}}^0 &= 2t_2 \cos\theta \left[\cos(\sqrt{3}k_x) + 2 \cos\left(\frac{\sqrt{3}}{2}k_x\right) \cos\left(\frac{3}{2}k_y\right) \right], & d_{\mathbf{k}}^1 &= t_1 \left[\cos k_y + 2 \cos\left(\frac{\sqrt{3}}{2}k_x\right) \cos\left(\frac{k_y}{2}\right) \right], \\ d_{\mathbf{k}}^2 &= t_1 \left[\sin k_y - 2 \cos\left(\frac{\sqrt{3}}{2}k_x\right) \sin\left(\frac{k_y}{2}\right) \right], & d_{\mathbf{k}}^3 &= M - 2t_2 \sin\theta \left[\sin(\sqrt{3}k_x) - 2 \sin\left(\frac{\sqrt{3}}{2}k_x\right) \cos\left(\frac{3}{2}k_y\right) \right], \end{aligned} \quad (22)$$

where t_1 and t_2 are nearest-neighbor and next-nearest-neighbor hopping amplitudes, θ is an additional effective phase of hopping between next-nearest-neighbor sites, and M is the staggered sublattice potential. For a finite lattice of size $N = L \times L$, the momenta are quantized as $k_x = \frac{2\pi m_x}{\sqrt{3}L}$, $k_y = \frac{4\pi m_y}{3L}$ with $m_{x(y)} = 1, 2, \dots, L$. The model is characterized by the Chern number \mathcal{C} . It undergoes topological quantum phase transitions at

$$M = \pm 3\sqrt{3}t_2 \sin\theta, \quad (23)$$

which separate a topologically non-trivial phase with $\mathcal{C} = \pm 1$ from a topologically trivial phase with $\mathcal{C} = 0$. For simplicity we set $t_1 = 1$, $t_2 = 1/2$ and $\theta = \pi/6$ in the following discussion. The critical points then lie at $M = \pm \frac{3\sqrt{3}}{4} \approx \pm 1.30$.

In order to explore fidelity zeros in the complex plane, we extend M into the complex domain $M = M_R + iM_I$. We first compute the minimum real part of the energy gap E_{\min} as a function of M in the complex plane, as shown in Fig. 3(a). A clear structural pattern similar to the case of Kitaev chain emerges. For $|M_R| \leq 1.30$ there is a region where $E_{\min}(M) = 0$, with boundaries indicated by the red closed curve and gray lines. Within this region, the real part of the energy gap closes for at least one momentum mode, satisfying the necessary condition for the appearance of fidelity zeros. In contrast, for $|M_R| > 1.30$, $E_{\min}(M)$ remains strictly positive, indicating that no spectral degeneracy in the real part occurs and hence fidelity zeros are absent. This sharp change in the behavior of $E_{\min}(M)$ across $|M_R| \approx 1.30$ again provides a direct link between the complex plane zeros and

the underlying quantum phase transition of the original Hermitian system.

For a finite-size system, we also analyze the distribution of fidelity zeros via the minimum single-mode fidelity defined in Eq. (7). Figure 3(b) shows $\mathcal{F}_{\min}(M + \delta M/2, M - \delta M/2)$ as a function of M , with fixed $\delta M = 0.01(1 + i)$. The dark blue lines are identified as fidelity zeros. These zeros are distributed along lines parallel to the imaginary axis. The exact positions of fidelity zeros can also be obtained analytically by requiring the energy gap to be pure imaginary, i.e., $\text{Re}(E_{\mathbf{k},+} - E_{\mathbf{k},-}) = 0$. Solving this condition yields explicit constraints on the complex parameter $M = M_R + iM_I$

$$M_R = -4t_2 \sin\left(\frac{\sqrt{3}}{2}k_x\right) \sin\theta \left[\cos\left(\frac{3}{2}k_y\right) - \cos\left(\frac{\sqrt{3}}{2}k_x\right) \right], \quad (24a)$$

$$M_I^2 \geq t_1^2 \left[3 + 2 \cos(\sqrt{3}k_x) + 4 \cos\left(\frac{\sqrt{3}}{2}k_x\right) \cos\left(\frac{3}{2}k_y\right) \right]. \quad (24b)$$

These constraints provide the locus of fidelity zeros for a given momentum \mathbf{k} . We verify these analytic expressions in Appendix A. Moreover, from the explicit expression for M_R in Eq. (24a), we can directly deduce its permissible range $|M_R| \leq 3\sqrt{3}t_2 \sin\theta$. This derived bound coincides precisely with the location of the topological quantum phase transition points in the original Hermitian Haldane model. This again indicates that for the Haldane model, fidelity zeros can appear only when the real part of the complexified parameter lies inside one phase (the

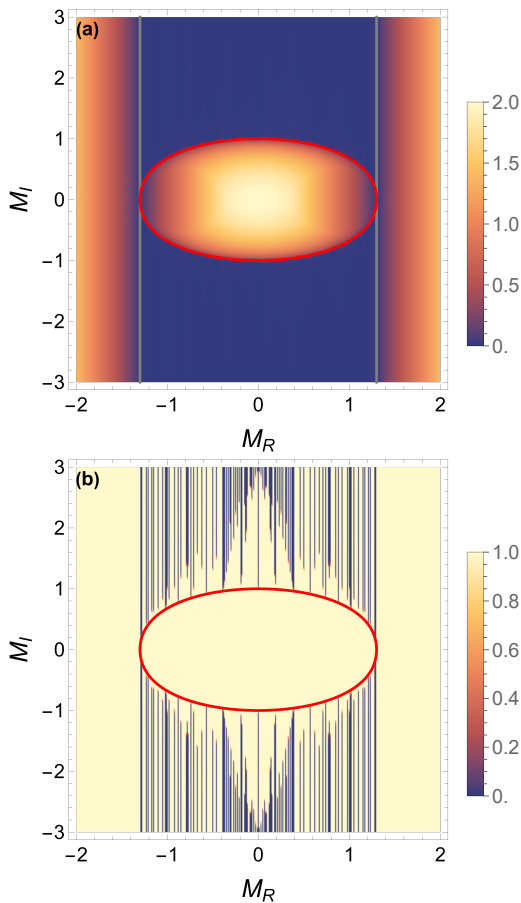


FIG. 3. (a) The minimum real part of the energy gap $E_{\min}(M)$ and (b) the minimum single-mode fidelity $\mathcal{F}_{\min}(M + \delta M/2, M - \delta M/2)$ as a function of M in the complex plane for the Haldane model. In panel (b) we fix $\delta M = 0.01(1 + i)$ and $L = 16$.

topologically non-trivial phase) of the original Hermitian model.

C. QWZ model

Finally, we consider the QWZ model [45], which is a two-dimensional two-band model described by the Hamiltonian Eq. (1) with components

$$\begin{aligned} d_{\mathbf{k}}^0 &= 0, & d_{\mathbf{k}}^1 &= \sin k_x, & d_{\mathbf{k}}^2 &= \sin k_y, \\ d_{\mathbf{k}}^3 &= u + \cos k_x + \cos k_y, \end{aligned} \quad (25)$$

where u is the staggered onsite potential. Depending on the value of u , this model has three different phases characterized by the Chern number \mathcal{C} : $|u| > 2$ with $\mathcal{C} = 0$, $-2 < u < 0$ with $\mathcal{C} = -1$, and $0 < u < 2$ with $\mathcal{C} = 1$. The energy spectrum is given by

$$E_{\mathbf{k},\pm} = \pm \sqrt{\sin^2 k_x + \sin^2 k_y + (u + \cos k_x + \cos k_y)^2}. \quad (26)$$

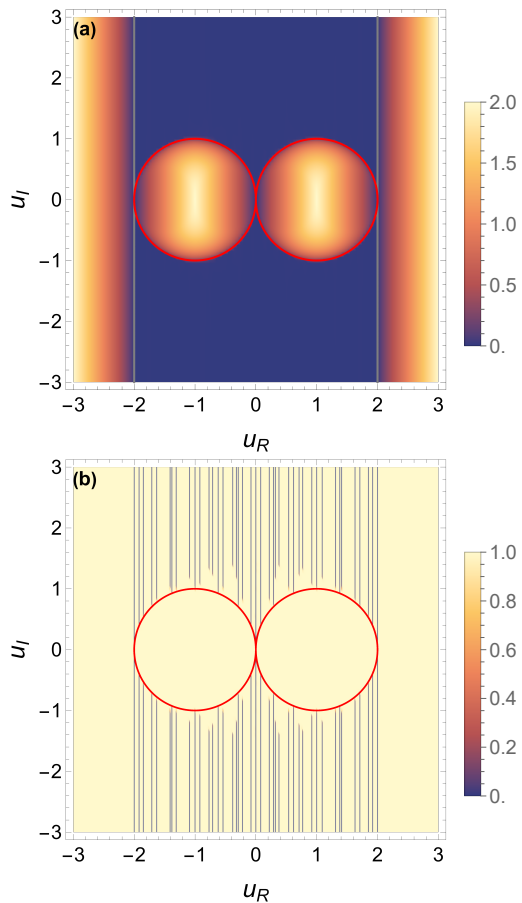


FIG. 4. (a) The minimum real part of the energy gap $E_{\min}(u)$ and (b) the minimum single-mode fidelity $\mathcal{F}_{\min}(u + \delta u/2, u - \delta u/2)$ as a function of u in the complex plane for the QWZ model. In panel (b) we fix $\delta u = 0.01(1 + i)$ and $L = 16$.

For a system of size $N = L \times L$, the allowed momenta are given by $k_{x(y)} = \frac{2\pi m_{x(y)}}{L}$ with $m_{x(y)} = 1, 2, \dots, L$.

We first compute the minimum real part of the energy gap $E_{\min}(u)$ of the QWZ model in the complex u -plane, as shown in Fig. 4(a). For $|u_R| \leq 2$, a region exhibiting $E_{\min}(u) = 0$ emerges, with red closed curves and gray lines indicating the boundaries. For $|u_R| > 2$, $E_{\min}(u)$ remains strictly positive, indicating the absence of fidelity zeros. Again, monitoring the existence of fidelity zeros as a function of u_R offers a diagnostic of the topological quantum phase transition at $u = \pm 2$. The critical point at $u = 0$ cannot be directly extracted from the existence or non-existence of fidelity zeros. However, fidelity zeros will cross the real axis at $u = 0$ in the thermodynamic limit, since the two red closed curves are tangent to each other at $u = 0$. Following the philosophy of the Lee-Yang theory, the zero approaching the real axis represents the critical point.

Next, we investigate the distribution of fidelity zeros for the QWZ model via the minimum single-mode fidelity. In Fig. 4(b) we plot $\mathcal{F}_{\min}(u + \delta u/2, u - \delta u/2)$ as a function of u , with fixed $\delta u = 0.01(1 + i)$. These zeros

again lie along lines parallel to the imaginary axis. We derive the exact positions of fidelity zeros, by requiring $\text{Re}(E_{\mathbf{k},+} - E_{\mathbf{k},-}) = 0$. Solving this condition yields explicit constraints on the complex parameter $u = u_R + iu_I$

$$u_R = -\cos k_x - \cos k_y, \quad (27a)$$

$$u_I^2 \geq 2 - \cos^2 k_x - \cos^2 k_y. \quad (27b)$$

Verification of these constraints is shown in Appendix A. From Eq. (27a) we can directly deduce $|u_R| \leq 2$, which precisely gives rise to the positions of critical points. For the QWZ model, although the critical point at $u = 0$ cannot be identified simply from the presence or absence of fidelity zeros, it is signaled by zeros approaching the real axis, mirroring the Lee-Yang paradigm of phase transitions.

IV. CONCLUSION

In summary, we have investigated fidelity zeros in two-band topological models by extending the phase transition driving parameter into the complex plane. We unveiled that fidelity zeros emerge precisely when the real part of the energy gap closes for certain momentum modes, thereby establishing a direct connection between fidelity zeros and the spectral properties of the corresponding non-Hermitian Hamiltonian. Using the Kitaev chain, the Haldane model, and the QWZ model as representative examples, we demonstrated that fidelity zeros exhibit universal distribution patterns. In finite-size systems, they appear as discrete lines parallel to the imaginary axis, with their real parts confined to a finite interval. Remarkably, the boundaries of the interval converge to the critical points of the underlying topological phase transitions in the thermodynamic limit. Our study extends the fidelity-zero framework to topological quantum phase transitions, demonstrating its effectiveness as a diagnostic tool beyond symmetry-breaking transitions.

ACKNOWLEDGMENT

This work is supported by National Key Research and Development Program of China (Grant No. 2023YFA1406704) and the NSFC under Grants No. 12474287, No. 12547107, and No. T2121001.

DATA AVAILABILITY

The data that support the findings of this article are not publicly available. The data are available from the

authors upon reasonable request.

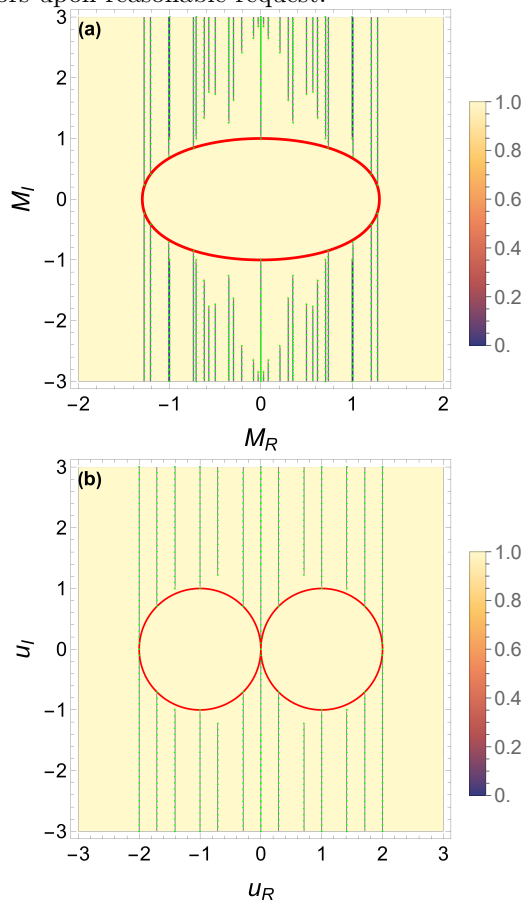


FIG. 5. Comparison between fidelity zeros computed from the analytic expressions (green dots) and those obtained numerically (dark blue lines), for (a) the Haldane model and (b) the QWZ model with $L = 8$.

Appendix A: Verification of analytic expressions for fidelity zeros

In this section, we verify the analytic expressions of fidelity zeros for the Haldane model [Eq. (24)] and the QWZ model [Eq. (27)]. In Fig. 5, The green dots are obtained using the analytic expressions, showing full agreement with the numerically obtained ones (dark blue lines).

[1] S. Sachdev, *Quantum Phase Transitions*, 2nd ed. (Cambridge University Press, 2011).

[2] P. Zanardi and N. Paunković, Ground state overlap and quantum phase transitions, *Phys. Rev. E* **74**, 031123

- (2006).
- [3] S.-J. Gu, Fidelity approach to quantum phase transitions, *International Journal of Modern Physics B* **24**, 4371 (2010), <https://doi.org/10.1142/S0217979210056335>.
 - [4] W.-L. You, Y.-W. Li, and S.-J. Gu, Fidelity, dynamic structure factor, and susceptibility in critical phenomena, *Phys. Rev. E* **76**, 022101 (2007).
 - [5] S. Chen, L. Wang, Y. Hao, and Y. Wang, Intrinsic relation between ground-state fidelity and the characterization of a quantum phase transition, *Phys. Rev. A* **77**, 032111 (2008).
 - [6] H.-K. Tang, M. A. Marashli, and W. C. Yu, Unveiling quantum phase transitions by fidelity mapping, *Phys. Rev. B* **104**, 075142 (2021).
 - [7] B.-B. Wei and X.-C. Lv, Fidelity susceptibility in the quantum rabi model, *Phys. Rev. A* **97**, 013845 (2018).
 - [8] G. Sun, B.-B. Wei, and S.-P. Kou, Fidelity as a probe for a deconfined quantum critical point, *Phys. Rev. B* **100**, 064427 (2019).
 - [9] B.-B. Wei, Fidelity susceptibility in one-dimensional disordered lattice models, *Phys. Rev. A* **99**, 042117 (2019).
 - [10] M. Heyl, A. Polkovnikov, and S. Kehrein, Dynamical quantum phase transitions in the transverse-field ising model, *Phys. Rev. Lett.* **110**, 135704 (2013).
 - [11] S. Vajna and B. Dóra, Disentangling dynamical phase transitions from equilibrium phase transitions, *Phys. Rev. B* **89**, 161105 (2014).
 - [12] F. Andraschko and J. Sirker, Dynamical quantum phase transitions and the loschmidt echo: A transfer matrix approach, *Phys. Rev. B* **89**, 125120 (2014).
 - [13] H. Yin, S. Chen, X. Gao, and P. Wang, Zeros of loschmidt echo in the presence of anderson localization, *Phys. Rev. A* **97**, 033624 (2018).
 - [14] G. Sun and B.-B. Wei, Dynamical quantum phase transitions in a spin chain with deconfined quantum critical points, *Phys. Rev. B* **102**, 094302 (2020).
 - [15] T. I. Vanhala and T. Ojanen, Theory of the loschmidt echo and dynamical quantum phase transitions in disordered fermi systems, *Phys. Rev. Res.* **5**, 033178 (2023).
 - [16] B. Zhou, Y. Zeng, and S. Chen, Exact zeros of the loschmidt echo and quantum speed limit time for the dynamical quantum phase transition in finite-size systems, *Phys. Rev. B* **104**, 094311 (2021).
 - [17] Y. Zeng, B. Zhou, and S. Chen, Dynamical singularity of the rate function for quench dynamics in finite-size quantum systems, *Phys. Rev. B* **107**, 134302 (2023).
 - [18] S. Ye, Z. Zhou, N. A. Khan, and G. Xianlong, Energy-dependent dynamical quantum phase transitions in quasicrystals, *Phys. Rev. A* **109**, 043319 (2024).
 - [19] S. Ye, N. A. Khan, and M. Sajid, Disentangling connection between static and dynamical phase transitions, *Phys. Rev. A* **111**, 042208 (2025).
 - [20] Y. Zeng and S. Chen, Relation between equilibrium quantum phase transitions and dynamical quantum phase transitions in two-band systems, *Phys. Rev. B* **112**, 064307 (2025).
 - [21] Z.-Y. Zheng, X. Liu, S. Lin, Y. Zhang, and S. Chen, Loschmidt echo zeros in finite-size quantum systems with linear quench, *Phys. Rev. B* **113**, L020301 (2026).
 - [22] Y. Zeng, B. Zhou, and S. Chen, Exact zeros of fidelity in finite-size systems as a signature for probing quantum phase transitions, *Phys. Rev. E* **109**, 064130 (2024).
 - [23] C. N. Yang and T. D. Lee, Statistical theory of equations of state and phase transitions. i. theory of condensation, *Phys. Rev.* **87**, 404 (1952).
 - [24] T. D. Lee and C. N. Yang, Statistical theory of equations of state and phase transitions. ii. lattice gas and ising model, *Phys. Rev.* **87**, 410 (1952).
 - [25] S.-Y. Kim, Yang-lee zeros of the antiferromagnetic ising model, *Phys. Rev. Lett.* **93**, 130604 (2004).
 - [26] T. Kist, J. L. Lado, and C. Flindt, Lee-yang theory of criticality in interacting quantum many-body systems, *Phys. Rev. Res.* **3**, 033206 (2021).
 - [27] P. M. Vecsei, J. L. Lado, and C. Flindt, Lee-yang theory of the two-dimensional quantum ising model, *Phys. Rev. B* **106**, 054402 (2022).
 - [28] P. M. Vecsei, C. Flindt, and J. L. Lado, Lee-yang theory of quantum phase transitions with neural network quantum states, *Phys. Rev. Res.* **5**, 033116 (2023).
 - [29] M. Sedik, J. M. Bhat, A. Dhar, and B. S. Shastry, Yang-lee zeros of certain antiferromagnetic models, *Phys. Rev. E* **110**, 014117 (2024).
 - [30] X.-Y. Ouyang, Q.-J. Ye, and X.-Z. Li, Complex phase diagram and supercritical matter, *Phys. Rev. E* **109**, 024118 (2024).
 - [31] M. Abdelshafy and M. Sedik, Yang-lee zeros of two-dimensional nearest-neighbor antiferromagnetic ising models: A numerical linked cluster expansion study, *Phys. Rev. B* **112**, 054445 (2025).
 - [32] P. M. Vecsei, J. L. Lado, and C. Flindt, Lee-yang formalism for phase transitions of interacting fermions using tensor networks, *Phys. Rev. B* **111**, 075134 (2025).
 - [33] T.-Y. Gu and G. Sun, Fidelity zeros and lee-yang theory of quantum phase transitions, *Phys. Rev. B* **113**, 014417 (2026).
 - [34] T.-Y. Gu and G. Sun, Non-hermitian symmetry breaking and lee-yang theory for quantum xyz and clock models (2025), [arXiv:2512.08687 \[quant-ph\]](https://arxiv.org/abs/2512.08687).
 - [35] D. C. Brody, Biorthogonal quantum mechanics, *Journal of Physics A: Mathematical and Theoretical* **47**, 035305 (2013).
 - [36] H. Jiang, C. Yang, and S. Chen, Topological invariants and phase diagrams for one-dimensional two-band non-hermitian systems without chiral symmetry, *Phys. Rev. A* **98**, 052116 (2018).
 - [37] G. Sun, J.-C. Tang, and S.-P. Kou, Biorthogonal quantum criticality in non-hermitian many-body systems, *Frontiers of Physics* **17**, 33502 (2021).
 - [38] Y.-C. Tzeng, C.-Y. Ju, G.-Y. Chen, and W.-M. Huang, Hunting for the non-hermitian exceptional points with fidelity susceptibility, *Phys. Rev. Res.* **3**, 013015 (2021).
 - [39] P. W. Anderson, Infrared catastrophe in fermi gases with local scattering potentials, *Phys. Rev. Lett.* **18**, 1049 (1967).
 - [40] P. W. Anderson, Ground state of a magnetic impurity in a metal, *Phys. Rev.* **164**, 352 (1967).
 - [41] A. Y. Kitaev, Unpaired majorana fermions in quantum wires, *Physics-Uspekhi* **44**, 131 (2001).
 - [42] W. P. Su, J. R. Schrieffer, and A. J. Heeger, Solitons in polyacetylene, *Phys. Rev. Lett.* **42**, 1698 (1979).
 - [43] W. P. Su, J. R. Schrieffer, and A. J. Heeger, Soliton excitations in polyacetylene, *Phys. Rev. B* **22**, 2099 (1980).
 - [44] F. D. M. Haldane, Model for a quantum hall effect without landau levels: Condensed-matter realization of the "parity anomaly", *Phys. Rev. Lett.* **61**, 2015 (1988).

- [45] X.-L. Qi, Y.-S. Wu, and S.-C. Zhang, Topological quantization of the spin hall effect in two-dimensional paramagnetic semiconductors, *Phys. Rev. B* **74**, 085308 (2006).